

Influence of compression and shear on the strength of Composite Laminates with Z-pinned Reinforcement

T. Kevin O'Brien
U.S. Army Research Lab
NASA Langley Research Center
Hampton, VA 23681

Ronald Krueger
National Institute for Aerospace
Hampton, VA 23681

ABSTRACT

The influence of compression and shear loads on the strength of composite laminates with z-pins is evaluated parametrically using a 2D Finite Element Code (FLASH) based on Cosserat couple stress theory. Meshes were generated for three unique combinations of z-pin diameter and density. A laminated plate theory analysis was performed on several layups to determine the bi-axial stresses in the zero degree plies. These stresses, in turn, were used to determine the magnitude of the relative load steps prescribed in the FLASH analyses. Results indicated that increasing pin density was more detrimental to in-plane compression strength than increasing pin diameter. Compression strengths of lamina without z-pins agreed well with a closed form expression derived by Budiansky and Fleck. FLASH results for lamina with z-pins were consistent with the closed form results, and FLASH results without z-pins, if the initial fiber waviness due to z-pin insertion was added to the fiber waviness in the material to yield a total misalignment. Addition of 10% shear to the compression loading significantly reduced the lamina strength compared to pure compression loading. Addition of 50% shear to the compression indicated shear yielding rather than kink band formation as the likely failure mode. Two different stiffener reinforced skin configurations with z-pins, one quasi-isotropic and one orthotropic, were also analyzed. Six unique loading cases ranging from pure compression to compression plus 50% shear were analyzed assuming material fiber waviness misalignment angles of 0, 1, and 2 degrees. Compression strength decreased with increased shear loading for both configurations, with the quasi-isotropic configuration yielding lower strengths than the orthotropic configuration.

INTRODUCTION

One of the most common failure modes for composite structures is delamination [1]. Recently, z-pins* have been proposed to provide through-thickness reinforcement to composite laminates [2-3]. Z-pins are pultruded rods of carbon fiber and epoxy matrix. The z-pins are ultrasonically inserted through the thickness of a laminated composite

* The generic term z-pin will be used throughout the paper versus the trade mark **Z-Fiber™** registered by Aztex Inc.

prepreg, which is then cured in an autoclave. This approach to through-thickness reinforcement offers an alternative to stitching, and can provide much higher areal densities of reinforcement [4]. Although the toughening properties of stitches, z-pins and similar structures have been studied extensively, only a few investigations have focused on the effect of z-pins on the in-plane properties of laminates. Steeves demonstrated that disruption in the alignment of the fibers in the composite leads to a significant reduction in the in-plane compressive strength [4]. The z-pins may cause significant misalignment of the fibers of the composite because the diameter of the z-pins (~ 280 to $510 \mu\text{m}$) is large relative to the diameter of the fibers ($\sim 7 \mu\text{m}$). Previously, Sun and coworkers studied the influence of shear loads on the uni-axial compression strength of composites by testing an off-axis unidirectional lamina and extrapolating the compression strength [5-6]. They found that the addition of small shear loads significantly reduce the compression strength of unidirectional composite lamina. In this study, the influence of additional shear loads, along with axial compression, on the strength of lamina in some commonly utilized laminates with z-pins will be evaluated parametrically.

BACKGROUND

The compression strengths of unidirectional fiber-reinforced composite lamina are much less than their corresponding tensile strengths. This is typically attributed to the mechanism of fiber micro-buckling where the fiber loses the local support of the surrounding matrix material. As shown in figure 1, micro-buckling initiates from an imperfection (fiber waviness with misalignment angle $\bar{\Phi}$,) that forms a kink band of width, w , and inclination angle, β . In order to better assess the influence of critical parameters on lamina compression strength, Fleck and Shu developed a finite element code called FLASH [7-9]. This FE code is based on a 2D general Cosserat couple stress theory that assumes the unidirectional composite lamina is a homogeneous anisotropic material that carries couple stress as well as classical Cauchy point stress. The constitutive response is deduced from a unit cell consisting of a fiber, represented by a linear elastic Timoshenko beam, embedded in a non-linear elastic-plastic matrix. The continuum theory was implemented within a two-dimensional finite element code that uses 6-noded triangular plane strain elements with 3 degrees of freedom at each node (two-displacements and one rotation corresponding to rotation of the fiber cross section). The finite element procedure is based upon a Lagrangian formulation of the finite deformation of the composite and can accommodate both geometric and material nonlinearities. The code models finite deformation using a Newton-Raphson incremental solution procedure with a modified Riks algorithm in the final stage to handle snap-back behavior associated with fiber micro-buckling. Boundary loading is piecewise proportional with a loading parameter, λ , for each loading stage [7].

The FLASH code assumes micro-buckling initiates from an imperfection in the form of fiber waviness. Inputs include lamina stiffness properties, normalized by the shear yield strength, (τ_y) and Ramberg-Osgood strain hardening law parameters (α, n). FLASH allows options for input of fiber misalignment angle due to fiber waviness either as (1) an elliptical patch of waviness, or (2) an arbitrary distribution of initial fiber waviness

through initial misalignment angle, $\bar{\phi}$, at the Gauss integration point for each element. The first option prescribes the elliptical patch along one edge of the unit cell, and hence, was not useful for this study with an embedded void to simulate a lamina with an embedded z-pin.

ANALYSIS FORMULATION

For this study, finite element meshes with the z-pin and surrounding resin rich regions simulated as voids were generated for three unique combinations of pin diameter and density. Geometric parameters used to generate the finite element meshes of the unit cells for different z-pin diameters and z-pin areal densities are shown in figure 2. Detailed descriptions of equations defining the unit cell dimensions are given in references 10 and 11. It was assumed that the fiber is completely surrounded by resin as shown in figure 3, and hence, the transverse dimension of the void, D'_z , was increased by 0.02 mm compared to the z-pin diameter, D_z . The unit cell parameters were determined from the average of values measured from micrographs taken from different specimens with z-pins (table 1). Meshes are shown in figure 4 for the small (0.28 mm) z-pin with 2% and 4% areal density and the large (0.508 mm) z-pin with 2% areal density. The size of the elements was varied to provide the greatest mesh refinement near the resin pocket, and in the region of greatest fiber misalignment. Carbon Epoxy material data, including the measured strain hardening parameters for the Ramberg-Osgood law, were used as input for the FLASH analyses (table 2). Input of an arbitrary distribution of the fiber misalignment in FLASH is possible. However, these data were not readily available. Hence, a uniform distribution of initial fiber misalignment angles from 0 to 10 degrees was prescribed in unit cells simulating lamina with embedded z-pins.

A laminated plate theory analysis was performed on three layups, subjected to either pure compression or equal compression and shear loading ($N_x = N_{xy}$), to determine the bi-axial stresses in the zero degree plies. Transverse (σ_{22}) and shear (τ_{12}) stresses in the zero degree plies were normalized by the axial compression stresses (σ_{11}) in the fiber direction to identify the relative magnitudes of the zero degree ply stresses for the three laminates analyzed (table 3). In order to perform a parametric study, these relative percentages of axial compression, transverse tension, and shear stresses in the zero degree plies were used to determine the magnitude of the relative load steps prescribed in the FLASH analyses as shown in table 4. The compression stress is gradually incremented by FLASH until it reaches the specified limit defined by the user ($\sigma_{11}/\tau_y = -1000$, where τ_y is the shear yield strength of the material). This limit was deliberately chosen to be well above the onset of fiber microbuckling to assure that the analysis reached the failure point and did not terminate prematurely. For the combined load cases, the other loads were incremented in the proportions shown in table 4.

Unit cells were analyzed for three load cases: (1) a pure axial compression load case, (2) a combined axial compression and 10% shear load case, and (3) a combined axial compression and 50% shear load case. Load and boundary conditions used in this study

for axial compression (figure 5) were identical to those used by Steeves and others [4,7]. However, appropriate load and boundary conditions had to be determined before simulating shear loading in FLASH. Ultimately, boundary conditions identical to those used for the simulation of axial compression loading cases were used for shear loading [10,11]. Further details for setting up models of unit cells with z-pins using FLASH are documented in reference 11.

ANALYSIS RESULTS

Figure 6 shows the compression strength, corresponding to the onset of fiber microbuckling, as a function of fiber waviness for the three z-pin configurations analyzed. Results indicated that increasing pin density was more detrimental to compression strength than increasing pin diameter. Figure 7 shows the technique used to calculate the misalignment angle, $\bar{\Phi}$, associated with z-pin insertion for the three unit cell geometries based on the geometric points used to generate the unit cell finite element meshes [11]. The z-pin insertion angle was greater for the smaller diameter pins than for the larger diameter pins. In figure 8, compression strength predictions for lamina with z-pins were plotted as a function of the total misalignment angle due to z-pin insertion and fiber waviness. This has the effect of offsetting the z-pin results along the horizontal axis by the amount of the initial misalignment due to z-pin insertion. FLASH results were also generated for lamina with no-z-pins by closing the void to create a new unit cell mesh [10]. As shown in figure 8, compression strengths of lamina without z-pins agreed well with a closed form expression derived by Budiansky and Fleck [12]. FLASH results for lamina with z-pins were consistent with the closed form results, and FLASH results without z-pins, if the initial fiber waviness due to z-pin insertion was added to fiber waviness in the material to yield a total $\bar{\Phi}$.

Figure 9 shows the stress-displacement plots and shear stress contours for the small pin 2% areal density configuration analyzed assuming three values of fiber waviness (0, 1 and 5 degrees). In the plots of stress versus displacement, the average stress along the lower left edge of the unit cell is plotted versus the displacement (normalized by the fiber diameter) at the lower left corner of the unit cell [8,11]. The $\bar{\Phi} = 0$ case reflects specimen response due to initial misalignment associated with z-pin insertion alone. Each stress-displacement plot has a maxima indicating the onset of an unstable event (fiber microbuckling) followed by a finite deformation as the kink band forms and grows. The shear stress contours are plotted at the final load step and mimic the region where kink band formation would be anticipated. This becomes increasingly more obvious for higher values of fiber waviness. Similar plots for the other configurations and loadings are shown in reference 10.

As shown in figure 10, the addition of 10% shear to the compression loading significantly reduced the lamina strength compared to pure compression loading predicted by the Budiansky and Fleck equation. The FLASH results with z-pins were still consistent with FLASH results without z-pins when the initial fiber waviness due to z-pin insertion was added to fiber waviness. As shown in figure 11, the addition of 50% shear to the

compression loading appeared to drastically reduce the lamina strength compared to pure compression loading predicted by the Budiansky and Fleck equation. However, the FLASH results with z-pins were no longer consistent with FLASH results without z-pins when including the initial misalignment angle due to z-pin insertion. The results for the 2% density small z-pin configuration slightly decreased with fiber waviness angle. However, the results for the other two configurations did not vary with fiber waviness angle. As shown in figure 12, the applied shear stress was close to, and in one case exceeded, the shear yield strength of the material (table 2). This is in contrast to the compression plus 10% shear case, also shown in figure 12, where the applied shear stresses were consistently lower than the shear yield strength. Hence, gradual shear yielding may be the failure mode for this compression plus 50% shear loading rather than kink band formation. As shown in tables 3 and 4, this load case corresponds to equal compression and shear loading on a cross-ply $[0/90]_s$ laminate. Hence, laminates without 45 degree plies may be more likely to fail by shear yielding than microbuckling.

Strength prediction for stiffener reinforced skin laminates under combined compression and shear loading

Two different stiffener reinforced skin configurations with z-pins were analyzed (figure 13). The first configuration consisted of an 8-ply $(45/0/-45/90)_s$ quasi-isotropic skin bonded to a stiffener with a 16-ply $(45/0/-45/90)_{2s}$ quasi-isotropic flange. The second configuration consisted of a 6-ply $(45/0/-45)_s$ orthotropic skin bonded to a stiffener with an 18-ply $(45/0/0/-45/0/45/0/-45/0)_s$ flange. For both configurations, the total 24-ply combined laminate where the skin meets the stringer flange was modeled with 2% areal density 0.28 mm diameter z-pins. A laminated plate theory analysis was performed for both 24-ply laminates using the carbon epoxy material properties in table 2. However, a lower value of E_{11} (143 Gpa) was used to better represent the compression lamina stiffness in the fiber direction. The applied net compression stress was specified and the corresponding stresses in the individual plies were calculated.

For the quasi-isotropic configuration, the ratio of the applied net compression stress to the compression stress in the zero degree plies was 0.392. As expected, the 24-ply unsymmetric orthotropic configuration exhibited compression and bending coupling resulting in the maximum zero degree ply stresses in the outermost zero-degree skin ply. For this ply, the ratio of the applied net compression stress on the laminate to the compression stress in the zero degree ply was 0.480. The laminate theory calculation was performed allowing the full bending deformation due to the coupling that arises from the unsymmetric skin-flange laminate. If, however, this bending deformation is constrained in the structural configuration, the constraint should be applied when performing the laminate theory analysis to estimate the zero degree ply stresses. Alternatively, the zero degree ply stresses could be obtained directly from a numerical analysis of the skin-stiffener region if the individual plies are modeled discretely.

Unidirectional compression strengths predicted from FLASH were multiplied by the appropriate factor for each configuration and loading to calculate predicted strengths for the skin/stiffener-flange laminates. For each configuration, six unique loading cases

ranging from $N_{xy}/N_x = 0$ to $N_{xy}/N_x = 0.5$, were assumed in the FLASH analysis assuming material fiber waviness misalignment angles of 0, 1, and 2 degrees. Table 5 shows the normalized zero degree ply stresses (axial, transverse, and shear) for the six loadings on the two stringer reinforced skin configurations analyzed. The axial compression stress in the zero degree plies is shown as -1000 times the shear yield strength, τ_y . The magnitude of the other normalized stress components are shown relative to the normalized compression stress. These relative magnitudes were used as input to the FLASH code for each load case studied.

Figure 14 shows the predicted quasi-isotropic skin/stiffener-flange laminate strengths, corresponding to the onset of microbuckling in the zero degree plies, as a function of the misalignment angle. Figure 15 compares the strength of the skin/stiffener-flange laminates for the quasi-isotropic and orthotropic skin/stiffener-flange laminates for $N_{xy}/N_x = 0.5$. Results indicate that the quasi-isotropic configuration should have lower strengths than the orthotropic configuration. Figure 16 shows the combined shear plus compression strength, σ_{ult} , normalized by the compression only strength, σ_{ultc} , as a function of the normalized loading, N_{xy}/N_x , for the quasi-isotropic skin/stiffener-flange laminate assuming three values of misalignment angle, 0, 1 and 2 degrees. Although the absolute strength is lower for laminates with larger misalignment angles (fig.14), the normalized strength reduction ($\sigma_{ult}/\sigma_{ultc}$) is slightly less for larger misalignment angles (fig.16). Figure 17 compares the combined shear plus compression strength, normalized by the compression only strength, as a function of the normalized loading, N_{xy}/N_x , for the quasi-isotropic and orthotropic skin/stiffener-flange laminates assuming a misalignment angle of one degree. Although the strength is lower for the quasi-isotropic laminates than the orthotropic laminates, the normalized strength reduction is slightly less for the quasi-isotropic laminates.

CONCLUSIONS

Increasing pin density was more detrimental to in-plane compression strength than increasing pin diameter. Compression strengths of lamina without z-pins agreed well with a closed form expression derived by Budiansky and Fleck. FLASH results for lamina with z-pins were consistent with the closed form results, and FLASH results without z-pins, if the initial fiber waviness due to z-pin insertion was added to the fiber waviness in the material to yield a total misalignment. Addition of 10% shear to the compression loading significantly reduced the lamina strength compared to pure compression loading. Addition of 50% shear to the compression indicated shear yielding rather than kink band formation as the likely failure mode. Two different stiffener reinforced skin configurations with z-pins, one quasi-isotropic and one orthotropic, were also analyzed. Six unique loading cases ranging from pure compression to compression plus 50% shear were analyzed assuming material fiber waviness misalignment angles of 0, 1, and 2 degrees. Compression strength decreased with increased shear loading for both configurations, with the quasi-isotropic configuration yielding lower strengths than the orthotropic configuration.

REFERENCES

1. O'Brien, T.K., "Fracture Mechanics of Composite Delamination," ASM Handbook, Vol.21, *Composites*, August, 2001, p.241-245.
2. Clarke, A., Greenhalgh, E., Meeks, C. and Jones, C., *Enhanced Structural Damage Tolerance of CFRP Primary Structures by Z-pin Reinforcement*, 44th AIAA SDM Conference, paper AIAA-2003-1679, Norfolk, VA, 2003.
3. Freitas, G., Fusco, T. and Campbell, T., *Z-fiber technology and products for enhancing composite design*. in *AGARD Conference Proceedings 590: Bolted/Bonded Joints in Polymeric Composites*. Advisory Group for Aerospace Research and Development, 1997, pp 8-17.
4. Steeves, C.A., *Mechanics of Failure in Composite Structures*, Ph.D. Dissertation, *Department of Engineering*, University of Cambridge: Cambridge, United Kingdom, 2001.
5. Sun, C.T. , *Novel Methods for Testing and Modelling Composite materials and Laminates*, Proceedings of the Second International Conference on Composites Testing and Model Identification, *CompTest 2004*, Bristol, England, September, 2004.
6. Sun, C.T. and Jun, A.W., *Compressive Strength of Unidirectional Composites with matrix non-linearity*, *Composites Science and Technology*, Vol. 52, No. 4, pp.577-587
7. Fleck, N.A. and Shu, J.Y., *Microbuckle Initiation in Fibre Composites: A Finite Element Study*, *J. Mechanics and Physics of Solids*, Vol.43, No.2, 1995, pp.1887-1918.
8. Shu, J.Y. and Fleck, N.A., *User's Manual for Finite Element Code for Fibre Microbuckling*, Cambridge University Engineering Department C-MATS Technical Report 224 (ISSN 0309-6505), May, 1995.
9. Liu, D. and Fleck, N.A., *User's manual II for Finite Element Code FLASH for Fibre Microbuckling*, Cambridge University Engineering Department C-MICROMECH Technical Report 29 (ISSN 0309-7420), November, 1999.
10. O'Brien, T.K., and Krueger, R.; *Influence of Compression and Shear on the strength of Composite Laminates with z-pinned reinforcement*, to be published as a NASA TM, 2005.
11. Krueger, R., *Modelling of unit-cells with z-pins using FLASH: Pre-processing and Post-processing*, NIA Report, 2005-01.
12. Budiansky, B. and Fleck, N.A., *Compressive Failure of Fibre Composites*, *J. Mechanics and Physics of Solids*, Vol.41, No.1, 1993, pp.183-211.

ACKNOWLEDGEMENTS

This research was supported by Sikorsky Aircraft and the U.S. Army Aviation Applied Technology Directorate under Technology Investment Agreement No. DAAH10-02-2-0001. The authors gratefully acknowledge Prof. Norman A. Fleck of Cambridge University, and Dr. Craig A. Steeves of Princeton University for providing the FLASH finite element code and insight into its use and application. The authors further acknowledge Dr. Jeffery Schaff of Sikorsky Aircraft for providing focus for the study.

Table 1

Carbon/Epoxy UD prepreg unit cell parameter dimensions

	2% areal density Large diameter	4% areal density small diameter	2% areal density small diameter
D_z	0.508 mm	0.28 mm	0.28 mm
D'_z	0.528 mm	0.3 mm	0.3 mm
H_z	3.18 mm	1.245 mm	1.753 mm
L_z	3.18 mm	1.245 mm	1.753 mm
C	2.18 mm	0.868 mm	0.868 mm

Table 2

Carbon epoxy material properties

E_{11}	161 GPa
E_{22} (tension)	11.4 GPa
E_{22} (compression)	12.8 GPa
G_{12}	5.17 GPa
G_f	22 GPa
τ_y	39 MPa
d	5.1 μm
V_f	0.59
ν_{12}	0.32
α	0.00923
n	8.54

Table 3. Normalized zero-degree ply stresses from laminate analysis

external load $N_x = -1000$ lbs/in			
Laminate	σ_{11}/σ_{11}	σ_{22}/σ_{11}	τ_{12}/σ_{11}
$[0/90]_s$	1	-0.02 (~2% σ_{11})	0
$[0/\pm 45]_s$	1	0.003 (~0% σ_{11})	0
$[0/45/-45/90]_s$	1	-0.0001 (~0% σ_{11})	0
external load $N_x = -1000$ lbs/in, plus $N_{xy} = -1000$ lbs/in			
	σ_{11}/σ_{11}	σ_{22}/σ_{11}	τ_{12}/σ_{11}
$[0/90]_s$	1	-0.02 (~2% σ_{11})	0.535 (~50% σ_{11})
$[0/\pm 45]_s$	1	0.003 (~0% σ_{11})	0.073 (~10% σ_{11})
$[0/45/-45/90]_s$	1	-0.0001 (~0% σ_{11})	0.085 (~10% σ_{11})

Table 4. FLASH input for load cases used for strength reduction analysis

	axial compression	compression 10% shear	compression 50% shear
σ_{11}/τ_y	-1000	-1000	-1000
σ_{22}/τ_y	-	-	-
τ_{12}/τ_y	-	100	500
τ_{21}/τ_y	-	100	500

Table 5 – Normalized zero degree ply stresses in skin/ stringer-flange laminates

Ply Stress	N_{xy}/N_x = 0	N_{xy}/N_x = 0.1	N_{xy}/N_x = 0.2	N_{xy}/N_x = 0.3	N_{xy}/N_x = 0.4	N_{xy}/N_x = 0.5
σ_{11}/τ_y	-1000	-1000	-1000	-1000	-1000	-1000
σ_{22}/τ_y	0	0	0	0	0	0
τ_{12}/τ_y	0	10	19	29	38	48

(A) Quasi-isotropic configuration

Ply Stress	N_{xy}/N_x = 0	N_{xy}/N_x = 0.1	N_{xy}/N_x = 0.2	N_{xy}/N_x = 0.3	N_{xy}/N_x = 0.4	N_{xy}/N_x = 0.5
σ_{11}/τ_y	-1000	-1000	-1000	-1000	-1000	-1000
σ_{22}/τ_y	35	35	35	34	34	34
τ_{12}/τ_y	0	10	20	30	40	50

(B) Orthotropic configuration

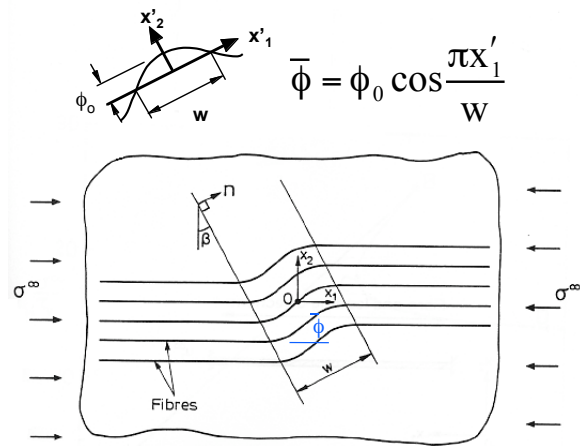


Figure 1. Fiber waviness parameters

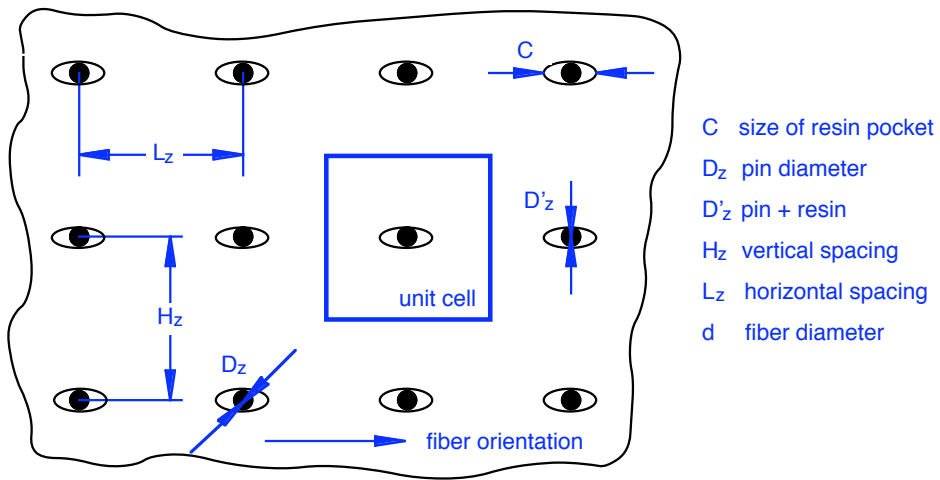


Figure 2. Z-pin geometric parameters

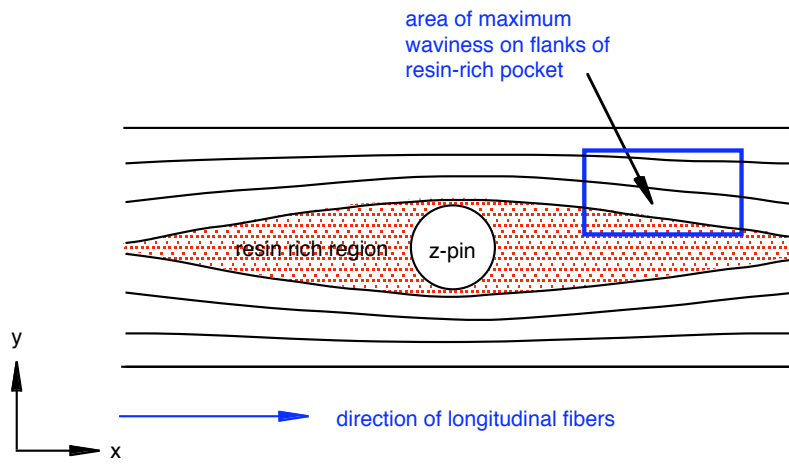
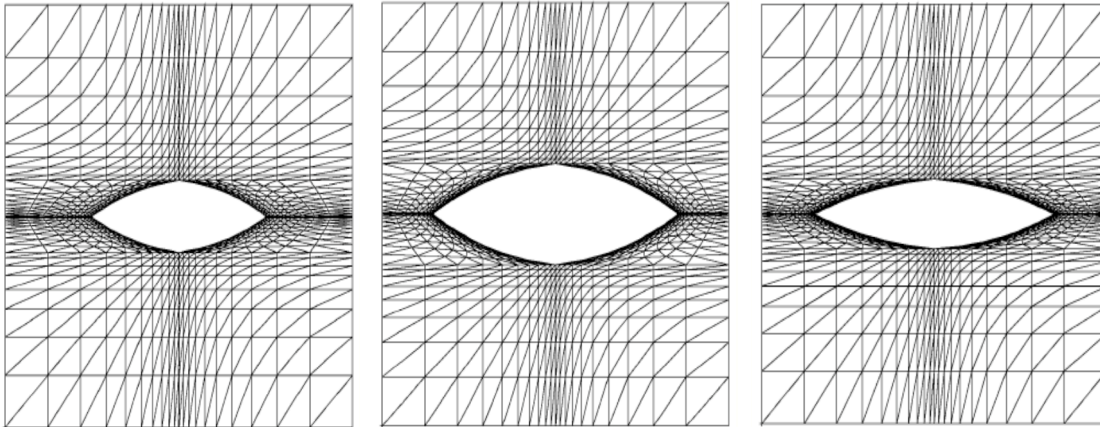


Figure 3. Fiber misalignment due to z-pin insertion



(A) 2% small z-pin (B) 4% small z-pin (C) 2% large z-pin

Figure 4. FLASH models of carbon epoxy lamina with embedded z-pins

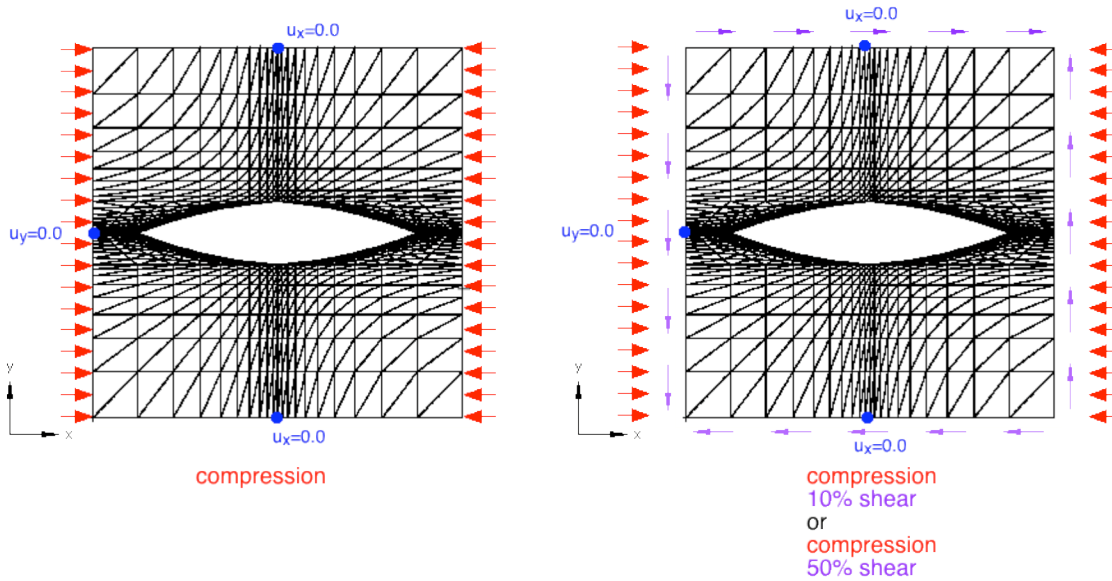


Figure 5. Loadings and prescribed displacements (u_x , u_y) on unit cells with z-pins [11]

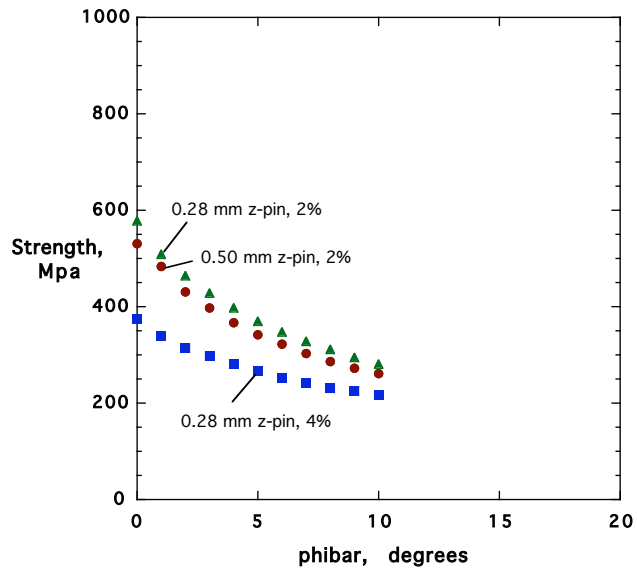


Figure 6. Influence of pin density and aerial weight percentage on compression strength

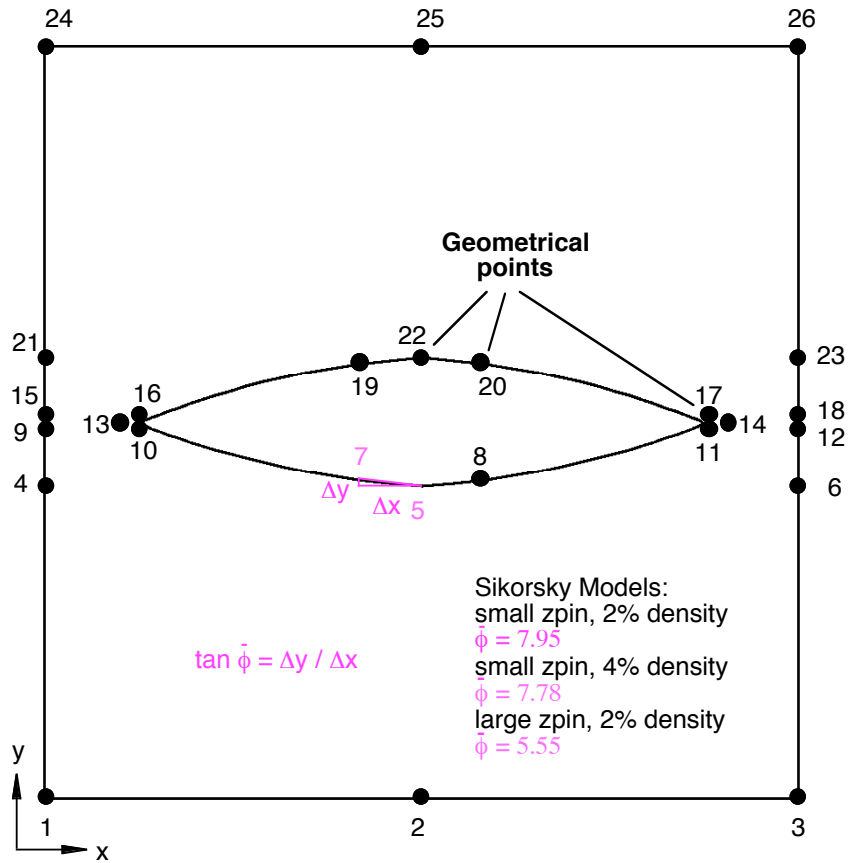


Figure 7. Calculation of fiber misalignment angle [11]

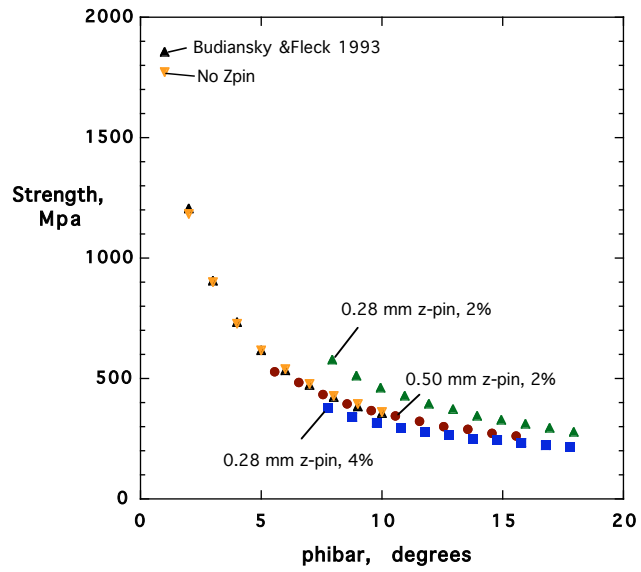


Figure 8. Predicted compression strengths with and without z-pins

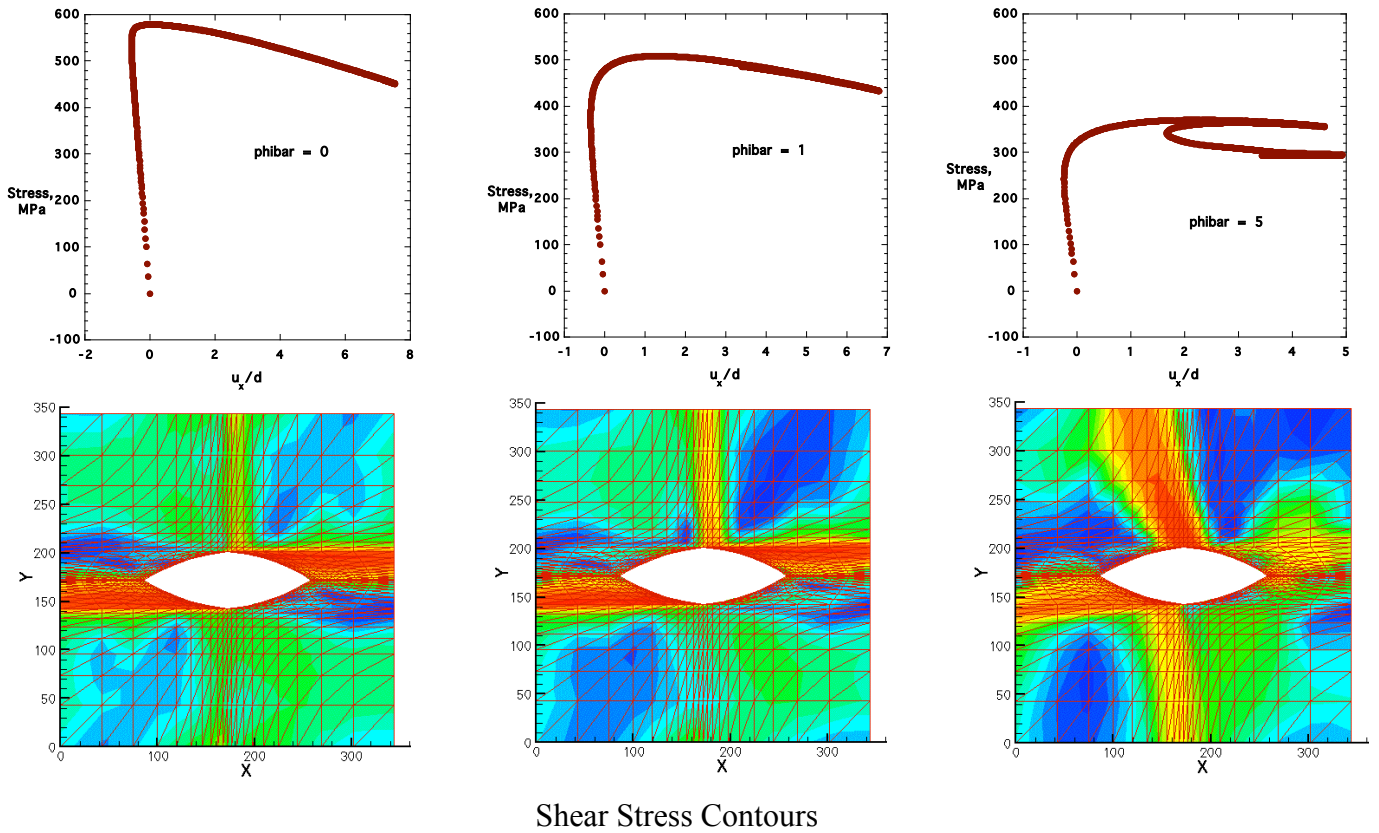


Figure 9. Influence of fiber waviness on response, small pin, 2% areal density

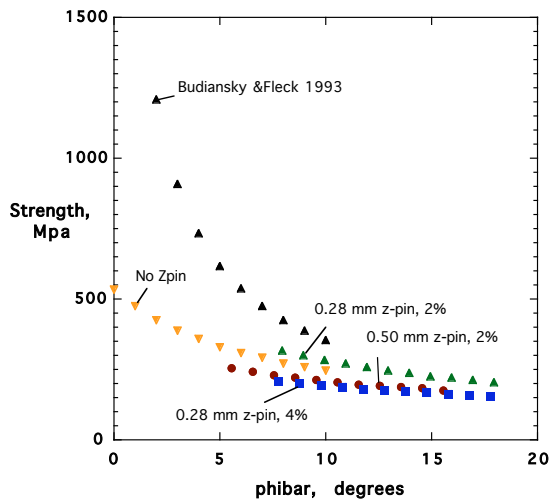


Figure 10. Predicted strengths for laminates with and without z-pins; compression plus 10% shear

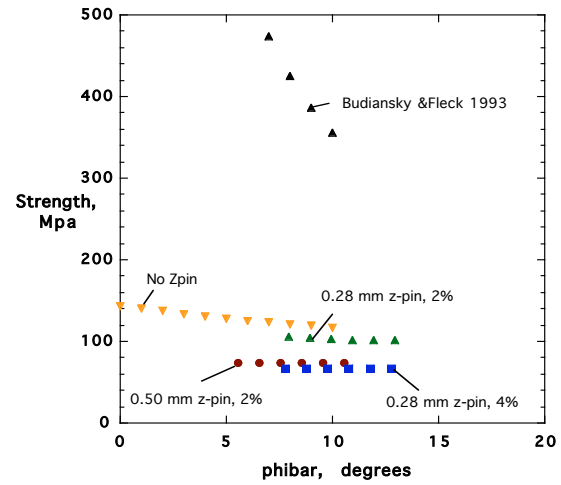


Figure 11. Predicted strengths for laminates with and without z-pins; compression plus 50% shear

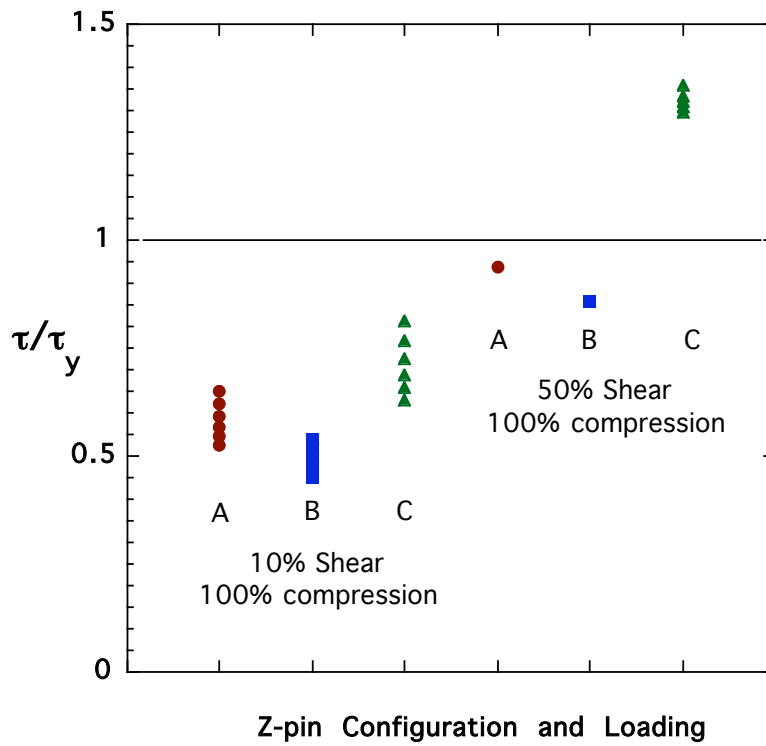


Figure 12. Ratio of applied shear stress at failure to shear yield strength of carbon epoxy

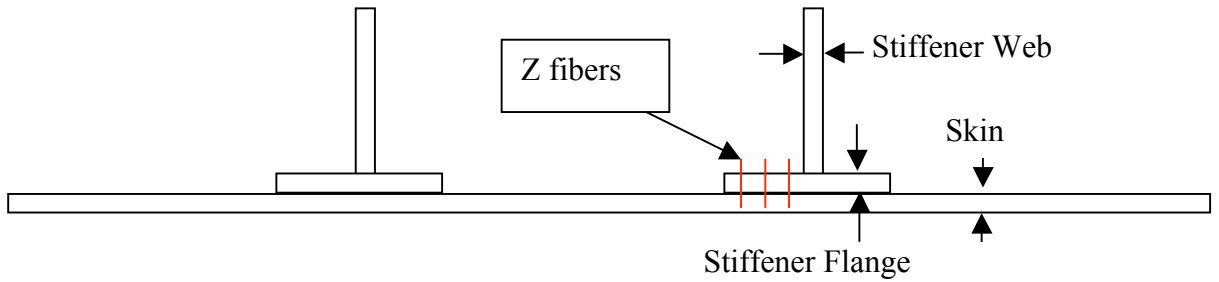


Fig.13 Stringer reinforced skin configurations

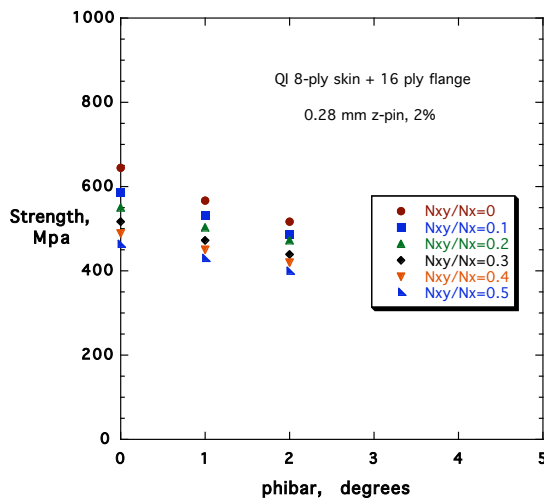


Fig.14 Skin/stiffener-flange laminate strengths for quasi-isotropic configuration

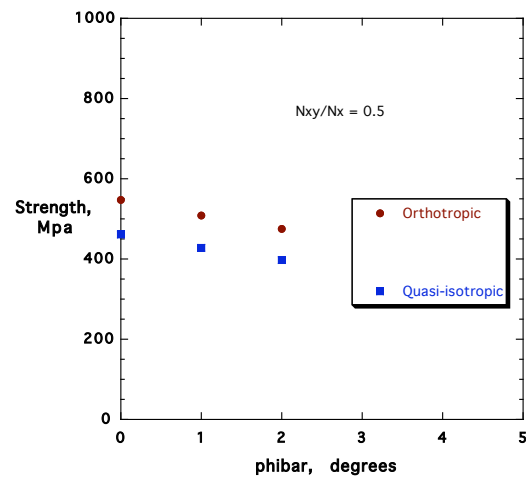


Fig.15 Comparison of quasi-isotropic and orthotropic laminate strengths

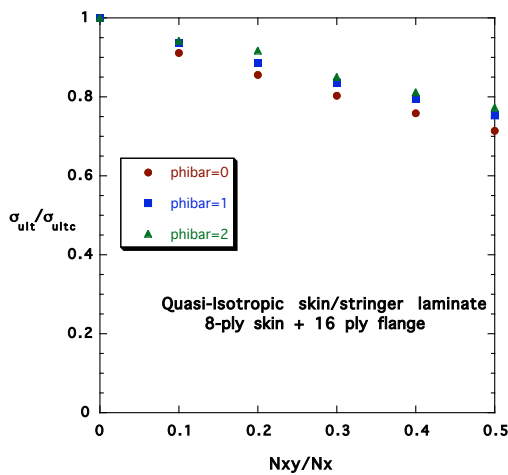


Fig.16 Normalized strength reduction for quasi-isotropic configuration

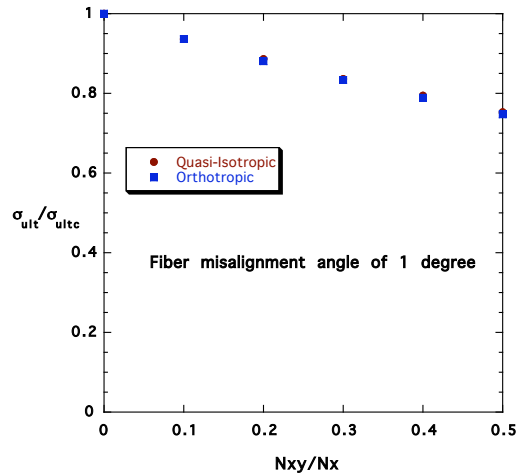


Fig. 17 Normalized compression strengths for QI and orthotropic configurations